Journal of Materials Science: Materials in Electronics (2019) 30:9582–9592
https://doi.org/10.1007/s10854-019-01292-2

Photo-stability of perovskite solar cells with Cu electrode

Abhishek K. Chauhan[1,2] · **Pankaj Kumar**[1,2]

Received: 24 November 2018 / Accepted: 6 April 2019 / Published online: 11 April 2019

Abstract
Towards higher stability of perovskite solar cells, Cu has been observed to be more suitable electrode material compared to conventional Al and Ag electrodes. The photo-stability of such devices has not been explored much in the literature, therefore we present here the investigation carried out towards the photo-stability of PSCs based on top Cu electrodes. The PSCs were prepared in normal geometry and stored in dark, under continuous illumination of a white LED lamp inside the laboratory and under direct sunlight outside the laboratory and tested as per the international summit on organic photovoltaics stability protocols. In dark storage the encapsulated solar cells exhibited highest stability but under illumination they exhibited degradation in their performance and the degradation was fastest in the direct sunlight. Degradation under illumination has been attributed to the photo-oxidation of the perovskite film. Cu has been observed to diffuse into and react with the underlying perovskite film and the ultraviolet and infrared contents in direct sunlight accelerated the photo-oxidation and chemical reactions between Cu and perovskite film. The chemical reactions of Cu electrode with perovskite constituents made it disappear after some time. These investigations suggest that Cu too is not a very stable electrode material for PSCs under natural operating conditions.

1 Introduction

Organo-metal halide perovskite semiconductors have shown enormous potential for efficient and cost effective conversion of solar energy into electricity and have now become the materials of high importance for energy conversion [1]. These materials have extraordinary electrical and optical properties and the power conversion efficiency (PCE) of perovskite solar cells (PSCs) has gone beyond 23% [2], approaching to that of the conventional Si solar cells. Integration of PSCs with Si solar cells in tandem structures has shown PCE over 26% [3–5] and it is expected that the PCE of such devices can easily go beyond 30% [6]. But before this technology is considered for real market products, its scalable fabrication and long term stability are the major issues that need to be sorted out. Usually PSCs are prepared via spin coating technique but some efforts have also been made to prepare perovskite films via well established scalable solution deposition techniques like spray coating [7], doctor blade coating [8], slot die coating [9] and screen printing [10]. Since PSCs incorporate the layers of multiple materials like light absorber, charge transport materials and electrodes, the process for large scale production of complete optimized structure is yet to be realized. Performance of PSCs is very sensitive to materials purities, processing conditions and growth methods. A little variation in these parameters leads to a very large variation in the device performance, so the performance is optimized very carefully. PSCs have shown to degrade and lose their photovoltaic properties at high temperatures and when exposed to oxygen, moisture and UV light [11–14]. It is observed that the water molecules hydrolyse the perovskites and break them into their precursors. For example, in the presence of H_2O molecules methyl ammonium lead iodide ($CH_3NH_3PbI_3$) breaks down into CH_3NH_3I (MAI) and lead iodide (PbI_2), while MAI further breaks down into CH_3NH_2 and HI [15, 16]. The decomposition of perovskites gets accelerated at high temperatures and in the presence of UV light [17]. Though the molecular decomposition can be overcome to some extent via molecular engineering [18–20], compositional engineering [21, 22] or using the cross linking additives in the precursors [23], but it is not only the perovskite materials that

✉ Pankaj Kumar
pankaj@nplindia.org

[1] Advanced Materials and Devices Metrology Division, CSIR-National Physical Laboratory, Dr. K. S. Krishnan Marg, New Delhi 110012, India

[2] Academy of Scientific and Innovative Research (AcSIR), Ghaziabad 201002, India

exhibit degradation, the charge transport layers, electrode materials and their interfaces with perovskite films also exhibit deterioration, which affect the overall performance of the devices.

Chemical reaction between perovskite and the electrode materials is the dominating degradation mechanism in PSCs. Aluminum (Al) and silver (Ag) are the most frequently used metals as electrodes in PSCs and both have shown strong chemical reactions with perovskites [24–26]. Introduction of metal oxide buffer layers or fullerenes between perovskite and metal electrodes has been observed to reduce the interfacial breakdown and degradation in PSCs [27–29]. But the actual solution of this problem would be to have an electrode material, which has high chemical resistivity against the perovskites. Though gold (Au) is less reactive compared to Al and Ag but it is too expensive to be used for large scale production. There are also some reports in the literature where copper (Cu) has been used as the top electrode [8, 30]. Cu has high corrosion resistance for non-oxidizing acids like HCl, HI, HBr and halogens [31]. Huang et al. replaced the top Al electrode by Cu in $CH_3NH_3PbI_3$ based PSCs in the inverted structure where solar cells were prepared on indium tin oxide (ITO) coated glass substrates in the ITO/poly[bis(4-phenyl)(2,4,6-trimethylphenyl)amine] (PTAA)/perovskite/indene-C_{60} bisadduct (ICBA)/C_{60}/2,9-dimethyl-4,7-diphenyl-1,10-phenanthroline (BCP)/metal cathode structure and studied for their air stability [8]. Interestingly, where the PCE of Al based solar cells dropped to zero just in 2 days, the solar cells based on Cu electrode showed almost zero loss for up to 30 days. These results clearly showed that Cu is less reactive to perovskite than Al. Less chemical reactivity of Cu with perovskite was also supported by X-ray diffraction (XRD) and cross-sectional scanning electron microscopic (SEM) studies [8]. It is worth noting that insertion of an electron transport layers between perovskite and Cu electrode would suppress the chemical reactions between them. In subsequent studies Huang et al. observed no chemical reaction between Cu and $CH_3NH_3PbI_3$ in encapsulated devices and predicted that at nominal operating cell temperature (NOCT) of 40 °C, the devices could be stable up to 22 years [30]. They observed no diffusion of Cu into perovskite for over 100 h at 80 °C. The solar cells retained 98% of their initial efficiency even after 816 h in ambient air without encapsulation. These studies show that Cu is a very stable electrode material for PSCs when devices are stored in ambient environment in dark, but not much detail is available on their photo-stability or stability under actual operating conditions. It would be very important to explore more about the suitability of Cu electrode for high stability in PSCs with different perovskite materials and charge transport layers.

We have investigated and report here the photo-stability of PSCs based on Cu electrode in indoor as well as actual outdoor conditions. The solar cells were not prepared in inverted structure like by Huang et al. [8, 30] but in the normal geometry on fluorine doped tin oxide (FTO) coated glass substrates with different charge transport materials. For detailed understanding of degradation mechanisms the solar cells were stored in different illumination conditions. Some of the solar cells were stored in dark, some were stored under continuous illumination of a white LED lamp and some were stored outside the laboratory under natural sunlight. The performance of devices was tested time to time as per the international summit on organic photovoltaic stability (ISOS) protocols [32]. Though the solar cells exhibited very high stability in dark storage but under illumination they indeed degraded and the degradation was very fast in actual outdoor conditions.

2 Experimental

2.1 Materials

Present investigation involved the use of FTO coated glass substrates, titanium iso-propoxide, titania paste (Dyesol 18NR-T), methyl ammonium iodide (MAI), lead iodide (PbI_2, 99%), phenyl C_{60} butyric acid methyl ester (PCBM), regioregular poly(3-hexylthiophene) (P3HT), Cu metal (99.99%), ethanol, anhydrous dimethyl formamide (DMF), anhydrous chloroform, acetone and isopropyl alcohol. Acetone, isopropyl alcohol and ethanol were purchased from MERCK Chemicals, Germany and MAI was purchased from Lumtech Chemicals, Taiwan. Other materials like FTO coated glass substrates, titanium iso-propoxide, titania paste, PbI_2, PCBM, P3HT, Cu metal, anhydrous DMF and anhydrous chloroform were purchased from Sigma Aldrich Chemicals, USA. All the materials were used as received from their sources.

2.2 Growth of perovskite films and characterization

Prior to solar cell fabrication, some of the thin films of perovskite material were subjected to the studies of their light absorption spectrum, crystal structure and surface morphology using UV–Vis absorption spectrometer (Shimadzu UV-2401 PC), X-ray diffractometer (XRD) (Cu Kα radiation, 1.54 Å) and Field Emission Scanning Electron Microscope (FE-SEM) (ZEISS, USA) respectively. The perovskite films were grown via spin coating of its precursor on the TiO_2 coated FTO substrates. It is worth mentioning here that the basic properties and growth of the perovskite crystals depend very strongly on the surface energy of the underlying films and the substrates [24]. Therefore to avoid any possible change, which might happen in morphology and other properties of the perovskite films due to variation

in the surface energy of the underlying film, all the perovskite films were grown on TiO_2-bl and TiO_2-mp coated FTO substrates only. Here TiO_2-bl represents the compact hole blocking, electron transport layer (ETL) of TiO_2 and TiO_2-mp represents the mesoporous ETL of TiO_2 nano-particles. This assured that the properties of the perovskite films in the solar cells were exactly the same as studied here. Prior to any deposition, the FTO substrates were properly cleaned via standard cleaning method. For compact TiO_2-bl films, mild acidic solution of titanium isopropoxide in ethanol was spin coated over FTO substrates at 2000 rpm for 60 s and cured at 300 °C for 5 min. Subsequently a dilute solution (80 mg/ml) of TiO_2 nano-particle paste (Dyesol 18NR-T) was spin coated at 2000 rpm for 30 s and annealed at 550 °C for 1 h in a muffle furnace. Both the TiO_2-bl and TiO_2-mp films were prepared in ambient environment. After cooling down to room temperature the samples were transferred to a glove box filled with high purity dry nitrogen ($O_2 < 1$ ppm, $H_2O < 1$ ppm), where perovskite films were grown via two steps method. First of all 400 mg/ml solutions of PbI_2 with 0.01 wt% of PCBM, dissolved in DMF, was spin coated over TiO_2-mp films at 6000 rpm for 60 s and annealed at 100 °C for 10 min. that yielded a pale yellow film of PbI_2. Since a minute amount of PCBM has been observed to improve the grain size of the perovskite crystals in thin films which in turn leads to enhanced short circuit current density (J_{sc}) and fill factor (FF) in solar cells [33, 34], we added 0.01 wt% of PCBM in PbI_2. After cooling down to room temperature 50 mg/ml solution of MAI in isopropyl alcohol was spin coated over PbI_2 films at 3000 rpm for 30 s and annealed at 100 °C for 30 min that resulted in conversion of the pale yellow films into dark brown films which was the indication of formation of perovskite crystals. The preparation of perovskite films is schematically shown in Fig. 1a. Finally these samples were used for the basic characterization of perovskite films via UV–Vis absorption, XRD and FE-SEM analysis.

2.3 Solar cell fabrication

The solar cells were prepared on FTO coated glass substrates in the configuration FTO/TiO_2-bl/TiO_2-mp/Perovskite/P3HT/Cu. FTO coated substrates were patterned and cleaned via standard cleaning procedure. In brief the substrates were sequentially cleaned with soap solution, distilled water, acetone and isopropyl alcohol. After cleaning the substrates were dried using high pressure dry nitrogen. Prior to any deposition the FTO substrates were treated with air plasma for 15 min in a vacuum chamber. The substrates were coated with TiO_2-bl and TiO_2-mp thin films in ambient

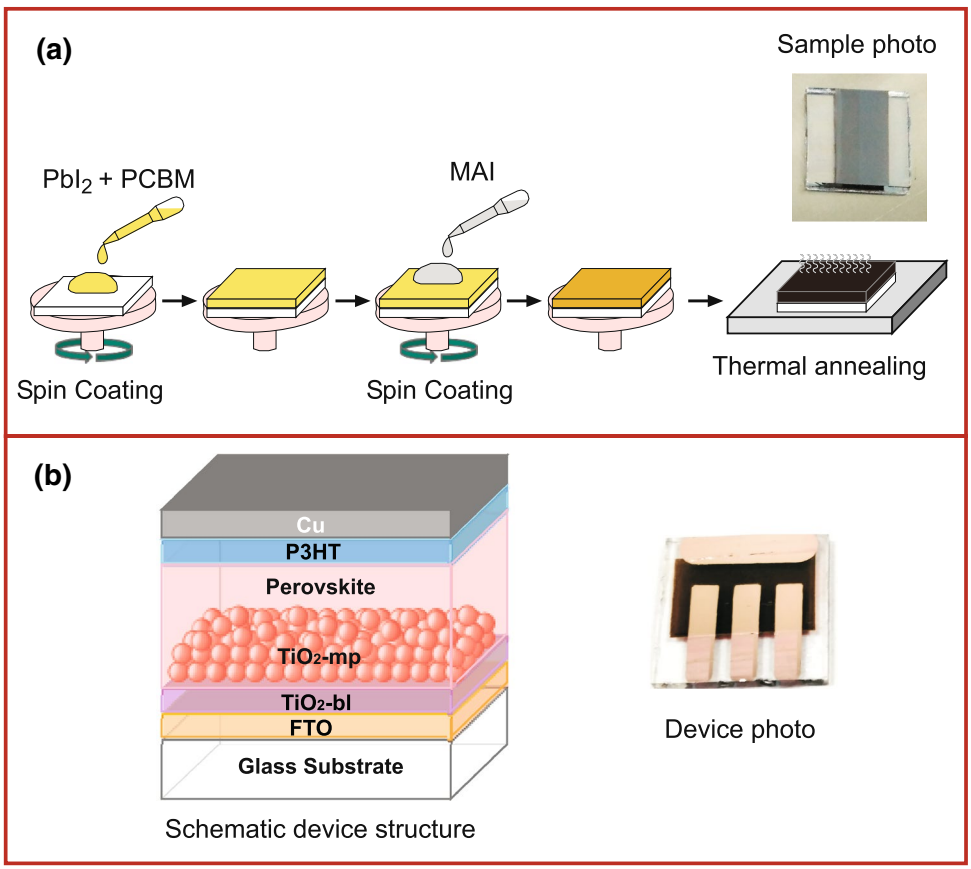

Fig. 1 **a** Schematic representation of the growth of perovskite films. **b** Schematic structure of the PSCs under study and a photograph of one of the solar cells

air following the procedure given in previous section. For the growth of perovskite films the samples were transferred to the glove box, where perovskite films were prepared following the method mentioned in previous section. For hole transport layer (HTL) 15 mg/ml solution of P3HT in anhydrous chloroform was spin coated at 4000 rpm for 60 s on the perovskite films. For the deposition of top Cu electrodes and to complete the solar cells, the samples were transferred to a vacuum chamber where 100 nm of Cu electrode was thermally evaporated onto the samples through a shadow mask at the base pressure of 2×10^{-6} mbar. The schematic structure and photograph of one of the solar cells is shown in Fig. 1b. It is worth mentioning here that in most efficient PSCs the HTL is usually a thin layer of Spiro-MeOTAD doped with *tert*-butylpyridine (TBP) and Lithium bis(trifluoromethanesulfonyl)imide (Li-TFSI) [35], but the hygroscopic nature of Li-TFSI leads to rapid degradation in cell performance in the moist environment [36]. Therefore the application of a more robust and stable HTL would result in better stability in PSCs. P3HT is an important HTL material which has shown very high stability in roll to roll polymer solar cells [37]. Keeping the stability of P3HT in our mind we used it as HTL in place of Spiro-MeOTAD. Since the hole mobility in P3HT is not as high as that in the doped Spiro-MeOTAD [38], the PCE of our solar cells was not as high as expected with doped Spiro-MeOTAD.

2.4 Solar cells characterization and storage

For determination of photovoltaic parameters, the solar cells were exposed to 100 mW/cm^2 illumination of an AM1.5G class AAA solar simulator from Photo Emission Tech (PET), USA and tested for their current density–voltage (*J–V*) characteristics under illumination using a Keithley 2400 Source Meter unit interfaced with a computer. The photovoltaic parameters were extracted out from the illuminated *J–V* characteristics that led us to calculate the PCE. The initial testing of solar cells was carried out in the air in ambient conditions and the devices were in air for quite some time. After initial measurements the cells were encapsulated in the glove box using glass cover slips and a UV curable epoxy from Epo-Tek, USA. Now for the understanding of degradation mechanisms, some of the solar cells were stored in dark, some were stored under continuous illumination of a white LED lamp at an irradiance of 10 mW/cm^2 and some were stored under natural sunlight outside the laboratory and their degradation studies were carried out as per the ISOS-D-1, ISOS-L-1 and ISOS-O-1 protocols respectively [32]. In brief, as per the ISOS-D-1 protocol the solar cells are stored in a dark chamber inside the laboratory with ambient conditions and tested periodically for their photovoltaic performance under solar simulator or natural sunlight. After testing the cells are stored back in the dark chamber. This procedure gives shelf life of the devices. As per ISOS-L-1 protocol the solar cells are stored under continuous illumination of a light source with constant illumination intensity inside the laboratory and tested periodically for their photovoltaic performance under solar simulator. This procedure gives the life time of devices under continuous indoor diffused light. As per ISOS-O-1 protocol the solar cells are stored in actual outdoor conditions under natural sunlight and tested periodically for their photovoltaic performance under solar simulator or natural sunlight. This procedure gives the actual lifetime of the devices in actual operating conditions.

3 Results and discussion

Figure 2a shows the X-ray diffraction (XRD) graph of $CH_3NH_3PbI_3$:PCBM film on TiO_2-bl/TiO_2-mp coated FTO glass substrate along with the XRD graphs of PbI_2:PCBM film on TiO_2-bl/TiO_2-mp coated FTO substrate and TiO_2-bl/TiO_2-mp coated FTO substrate only. The XRD pattern of FTO/TiO_2-bl/TiO_2-mp sample exhibited the diffraction peaks at 2θ values of 26.6°, 33.9°, 37.9°, 51.6°, 61.7° and 65.7° whereas the FTO/TiO_2-bl/TiO_2-mp/PbI_2:PCBM sample exhibited the diffraction peaks at 2θ values of 12.8°, 26.6°, 33.9°, 37.9°, 51.6°, 61.7° and 65.7°. The diffraction peak at 12.8° corresponds to (001) plane of hexagonal structure of PbI_2 and the other peaks correspond to the base substrate having TiO_2 and FTO. In case of FTO/TiO_2-bl/TiO_2-mp/$CH_3NH_3PbI_3$:PCBM sample the diffraction peaks occurred at 2θ values of 14.2°, 24.6°, 26.6°, 28.6°, 32.1°, 33.9°, 37.9°, 40.7°, 43.2°, 51.6°, 61.7° and 65.7°. The peaks at 14.2°, 24.6°, 28.6°, 32.1°, 40.7°, and 43.2° correspond to the (110), (202), (220), (310), (224) and (314) planes of $CH_3NH_3PbI_3$ perovskite whereas the other peaks correspond to base substrate having TiO_2 and FTO. The existence of (110), (202), (220), (310), (224) and (314) planes indicate the formation of highly crystalline tetragonal phase of $CH_3NH_3PbI_3$ perovskite. It is observed that addition of PCBM in PbI_2 has no effect on the crystal structure and diffraction peaks of the perovskite [33, 39]. Chiang et al. observed that pure and PCBM doped perovskite films have similar crystalline domain size but higher crystallinity in PCBM doped film [39]. PCBM does not react with any of the perovskite constituents or occupy any of the sites in the crystal lattice and does not affect the crystal structure but it interacts with perovskite precursor and helps in growth of perovskite crystals during thermal annealing. It plays an important role in crystal nucleation and increases the range of crystal growth leading to larger crystal gains [39]. Figure 2b shows the UV–Vis absorption spectra of PbI_2:PCBM and $CH_3NH_3PbI_3$:PCBM films on FTO/TiO_2-bl/TiO_2-mp substrates. The dotted lines at the absorption edge have

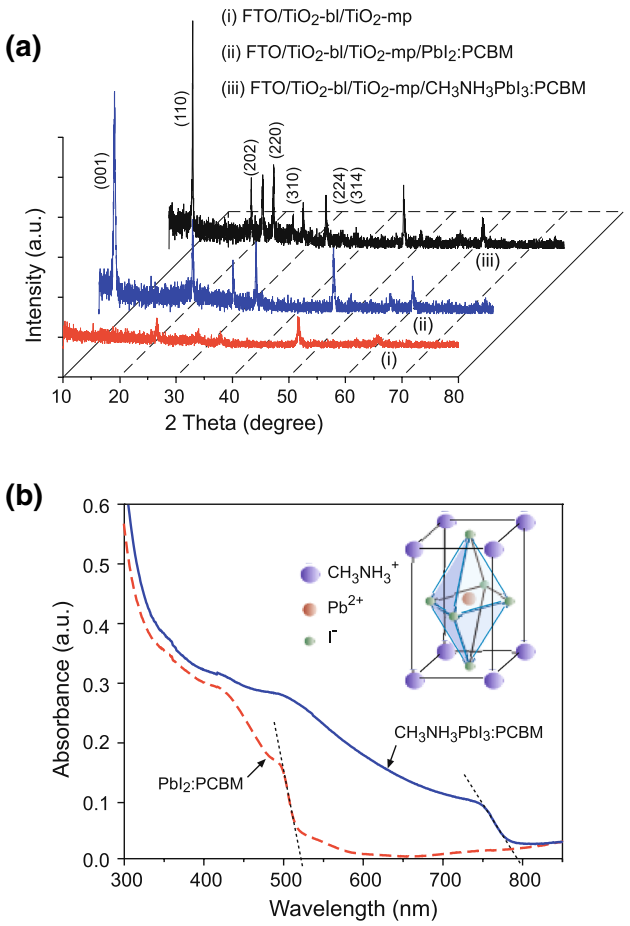

Fig. 2

Fig. 2 **a** XRD patterns of (i) FTO/TiO_2-bl/TiO_2-mp (ii) FTO/TiO_2-bl/TiO_2-mp/PbI_2:PCBM and (iii) FTO/TiO_2-bl/TiO_2-mp/$CH_3NH_3PbI_3$:PCBM structures. **b** UV–Vis absorption spectra of PbI_2:PCBM and $CH_3NH_3PbI_3$:PCBM thin films. The inset shows schematically the tetragonal crystal structure of $CH_3NH_3PbI_3$ perovskite

been plotted to extrapolate the low energy linear part of the absorption graphs to zero absorption to calculate the corresponding band gaps as per the Tauc relation. In this way the band gaps of the two materials were found to be 2.3 eV for PbI_2 and 1.58 eV for the $CH_3NH_3PbI_3$. Inset of Fig. 2b shows schematically the tetragonal structure of $CH_3NH_3PbI_3$ perovskite.

Figure 3 shows the scanning electron microscopic (SEM) images of the PbI_2:PCBM and $CH_3NH_3PbI_3$:PCBM films grown on the FTO/TiO_2-bl/TiO_2-mp substrates. Formation of PbI_2 crystals with some minute pin holes can be seen very clearly from the SEM image. The film was very uniform with high substrate coverage. When MAI was coated on PbI_2 film to form the perovskite, the pin holes were filled giving a very compact and uniform film of the perovskite with almost 100% substrate coverage. Higher substrate coverage results in reduced leakage current which in turn leads to higher open circuit voltage (V_{oc}) and *FF* [40, 41]. Low substrate coverage would cause HTL to be in contact with ETL that would result in enhanced recombination of photo-generated electrons with photo-generated holes. Enhanced recombination is reflected in poor shunt resistance of the devices. Additionally the uncovered area would cause incident photons to pass through without getting absorbed and contributing to photo-current. As a whole the low substrate coverage results in poor photovoltaic performance of the solar cells. Figure 4 shows the *J*–*V* characteristics of one of the perovskite solar cells. The characteristics were measured via scanning the voltage between − 0.2 and 1.1 V with step of 12 mV and measuring the corresponding current in both the forward and reverse sweeps. Inset shows the photovoltaic parameters of the solar cell calculated from forward and reverse sweep characteristics. The characteristics exhibited negligible hysteresis. The PCE of these devices has been observed to be lower than those incorporating Spiro-MeOTAD as HTL. Though the V_{oc} of these devices was very high ~ 1 V, the lower PCE was mainly because of lower J_{sc} and *FF*. Lower J_{sc} and *FF* in these devices can be clearly attributed to lower hole mobility through P3HT compared to Spiro-MeOTAD [38]. It is a well known fact that the HTL with lower hole mobility will introduce additional series resistance in the devices for collection of holes, that

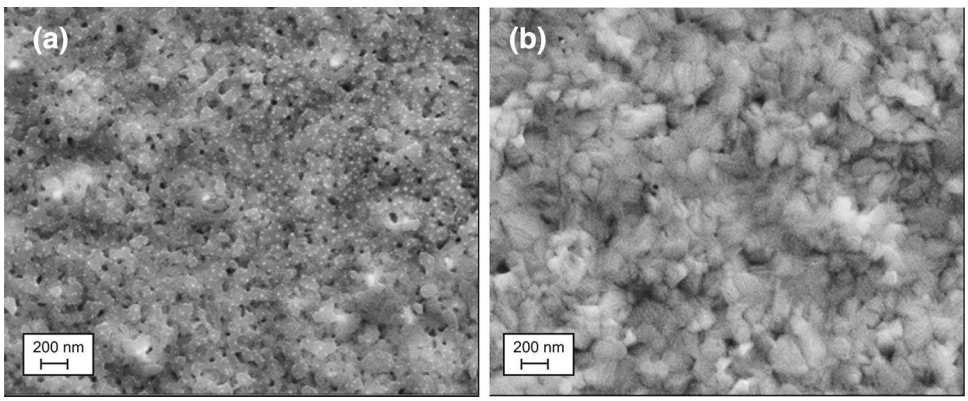

Fig. 3 SEM images of **a** PbI_2:PCBM and **b** $CH_3NH_3PbI_3$:PCBM thin films on the TiO_2-bl and TiO_2-mp coated FTO substrates

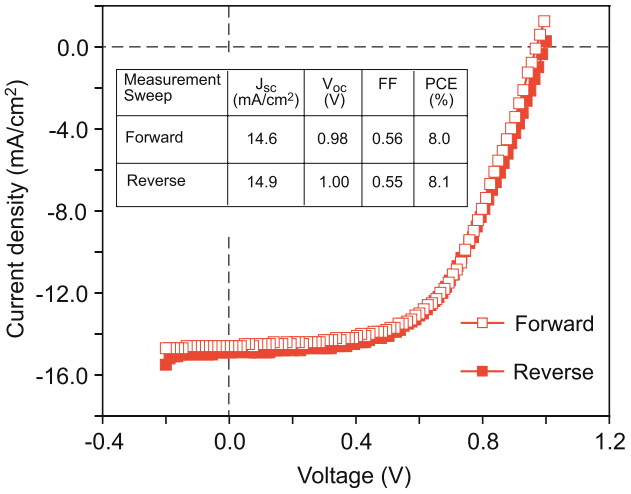

Fig. 4 *J–V* characteristics of one of the solar cells in forward and reverse sweeps. Inset shows that corresponding photovoltaic parameters

would cause enhanced recombination of charge carriers and reduced J_{sc} and *FF* [32].

Figure 5 shows the degradation profiles in the photovoltaic parameters of the solar cells tested as per the ISOS-D-1, ISOS-L-1 and ISOS-O-1 protocols. The devices were tested up to around 800 h. The values of the parameters were normalized with respect to the corresponding average value for three devices. In the dark storage and testing as per the ISOS-D-1 protocols, the temperature and relative humidity of the surrounding environment were 24 ± 4 °C and 45 ± 5% respectively. The solar cells were tested time to time for their photovoltaic performance and placed back in the dark after every measurement. The storage in dark environment had no significant effect on the performance of solar cells. However the PCE improved slightly in the initial hours and that was mainly because of slight improvement in J_{sc}. This improvement in J_{sc} can be attributed to reduced charge traps, reorganization of interlayer interfaces and healing effects with time in the perovskite films [42]. Reduction in

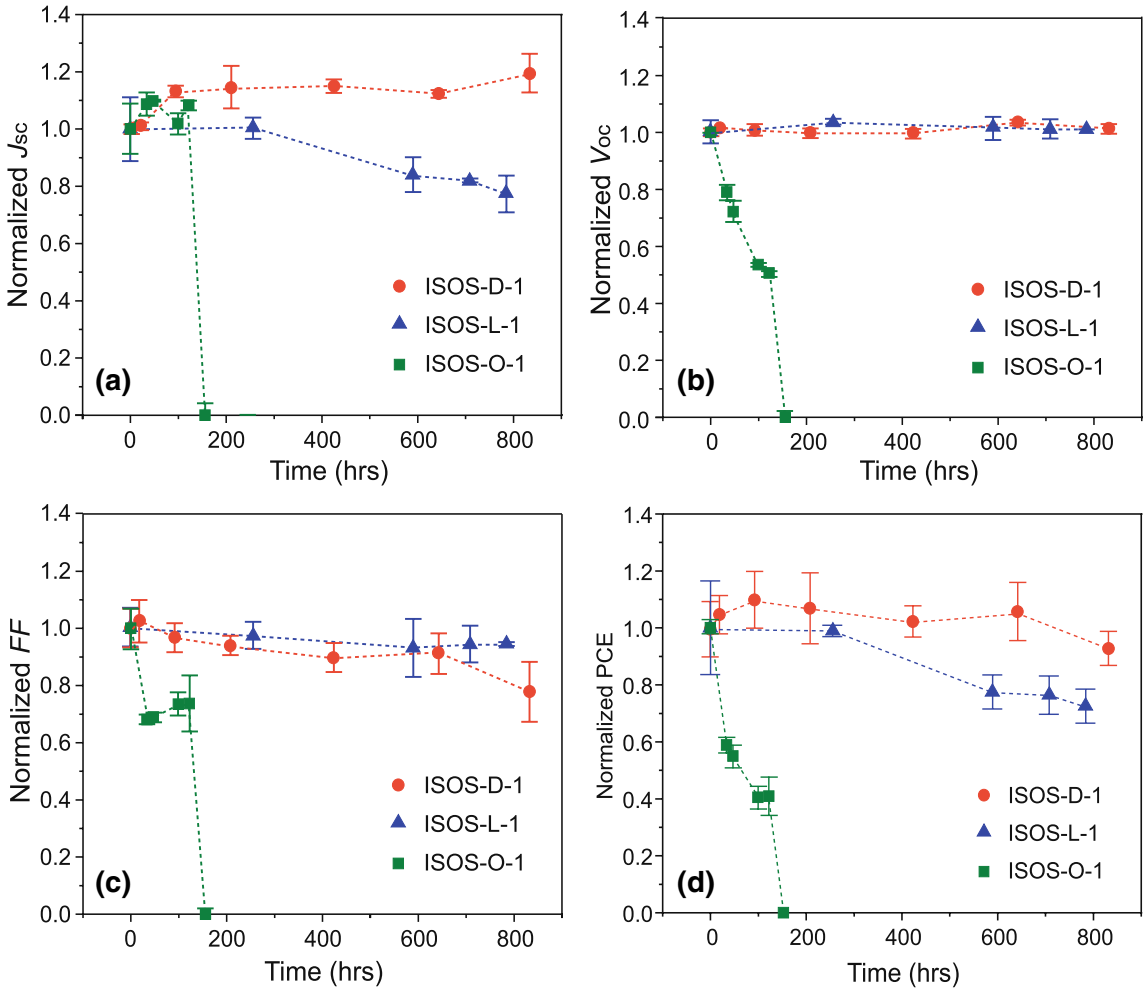

Fig. 5 Degradation profiles of normalized J_{sc}, V_{oc}, *FF* and PCE of the solar cells stored in different conditions and tested as per the ISOS-D-1, ISOS-L-1 and ISOS-O-1 protocols

charge traps would cause reduction in recombination losses and enhancement in the output current. Zhou et al. reported a reversible healing effect on the perovskite films via water molecules [42]. Though the sealed devices stored in dark are expected to be highly stable with no change in their photovoltaic performance but it is worth mentioning here that before encapsulation the devices were in air for quite some time for initial measurements. This resulted in exposure of the solar cells to ambient O_2 and H_2O molecules. Adsorption of O_2 and H_2O molecules during initial hours would have contributed to healing of the perovskite film and the effect of which was observed in the subsequent measurements. The encapsulation ensured no further diffusion of O_2 and H_2O molecules into the devices and contributed to reduction in subsequent degradation rate. We did not observe any change in V_{oc} of the cells but the *FF* reduced slightly. It is worth mentioning here that in the metal-insulator-metal (MIM) structures the difference in the work-function of the electrodes determines the built-in potential in the devices and built-in potential plays an important role in controlling the V_{oc} [43]. No deterioration in the V_{oc} of the cells suggests no deterioration in Cu electrode and no chemical reaction with perovskite film. However the reduction in *FF* can be attributed to interlayer interfacial changes. Please note that encapsulation inhibits the diffusion of external entities like O_2 and H_2O into the devices (depending upon the quality of barrier film and the encapsulating glue) but it does not prevent the internal inter-diffusion of constituent materials and interlayer interfacial changes that will affect the device performance. We also took photographs of the cells time to time from a digital camera and did not observe any visual defects or changes in the devices. Figure 6 shows photographs of some of the solar cells stored under different conditions. The photographs were taken at different time intervals but only the photographs for initial and final measurements are shown. High stability in dark storage is in agreement with the observations of Huang et al. [8, 30].

In case of storage under continuous illumination of a white LED lamp and testing as per the ISOS-L-1 protocols, the illumination intensity of the lamp was 10 mW/cm^2 and the temperature and humidity of the surrounding environment were 24 ± 4 °C and 45 ± 5% respectively. The solar cells were tested time to time for their photovoltaic performance and placed back under continuous illumination after every measurement. Continuous illumination from LED lamp caused little degradation in PCE of the cells with time and this degradation was mainly because of degradation in J_{sc} and *FF*. The V_{oc} exhibited no degradation with time and suggests no deterioration in electrode materials. We did not observe any visual defects or changes in the devices under continuous illumination of LED lamp (Fig. 6b). The illumination intensity of the lamp was 10 mW/cm^2 only. The degradation in performance was mainly because of internal

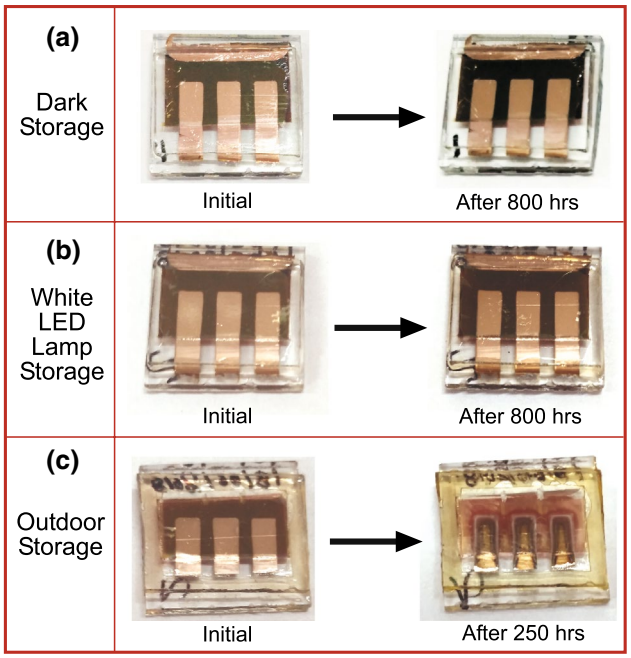

Fig. 6 Photos of some of the solar cells stored in **a** dark, **b** white LED lamp illumination and **c** outdoor conditions. The photos were taken time to time during investigation but only the photos of initial and final measurements are shown here

degradation in the device constituents, mainly the active layer. The reduction in J_{sc} and *FF* can be attributed to photo-degradation of the perovskite films. It is worth mentioning here that the organo-metal halide perovskite semiconductors exhibit photo-degradation, though the rate of degradation would depend upon the intensity and severity of the incident light [24]. Photo-degradation causes the perovskite films to decompose into its constituents and lose their optical and electrical properties. Loss in optical and electrical properties of perovskite would cause deterioration in J_{sc} and *FF* of the solar cells. These results suggested Cu electrode to be very stable even under mild illumination of a white LED lamp.

In case of sample storage under natural sunlight outside the laboratory and testing as per the ISOS-O-1 protocols, we observed very rapid and severe degradation in V_{oc} and *FF*. Though J_{sc} exhibited little improvement in initial few hours but after around 120 h it decreased very quickly and became zero. The reduction in V_{oc} and *FF* overcame the increment in J_{sc} and the overall PCE decreased with time. It is important to note that the degradation mechanisms of solar cells under natural sunlight were completely different from those under LED lamp illumination and the reason behind that was more harsh environmental conditions outside the laboratory. The outdoor illumination intensity was more than that of LED lamp and the solar radiation exhibited high ultraviolet (UV) and infrared (IR) radiations compared to that of LED lamp. The spectra of solar radiation and LED lamp are compared

in Fig. 7. During day time the environmental temperature varied from 25 to 42 °C and the humidity varied from 32 to 48%. The temperature and humidity were measured using the temperature and humidity sensors. During night the temperature went down to 16 °C and the humidity went up to 62%. The illumination intensity outside the laboratory was measured using a solar power meter from TENMARS, Taiwan and it varied from 0 in the night to ~ 95 mW/cm^2 at the noon. Since the devices were encapsulated using the glass cover slips the effect of humidity variation during testing is expected to be negligible but high temperature and high illumination intensity would contribute to rapid degradation in solar cell performance. The measurements of photovoltaic parameters were carried out during day time inside the laboratory. After each measurement the solar cells were placed back in the natural conditions outside the laboratory. The improvement in J_{sc} in initial hours was fluctuating and can be attributed to the recovery in the perovskite film during night [44]. During day time under continuous illumination of the solar light, J_{sc} decreased but during night it recovered. We did not see any improvement in J_{sc} for the studies as per ISOS-L-1 protocols and the reason behind that was continuous illumination of LED lamp for all the time. But more importantly the V_{oc} and *FF* exhibited very severe degradation and the reason behind that was reaction of Cu electrode with underlying materials. We could visually see the defects and changes happening in the solar cells. The top Cu electrode reacted with underlying materials and disappeared after some time (Fig. 6c). These results were very surprising as Cu was expected to be very stable material for PSCs [30], but it reacted with perovskite film and led to very rapid degradation in cell performance under natural operating conditions.

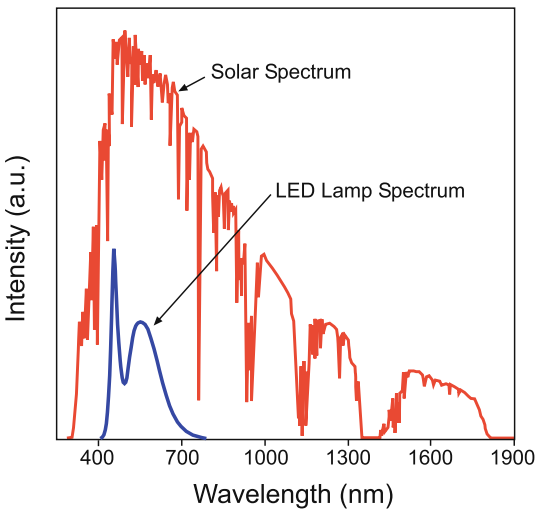

Fig. 7 Comparison of the solar spectrum corresponding to AM1.5G solar irradiance outside the laboratory with the spectrum of white LED lamp used in the present studies. The solar spectrum possessed UV and IR contents which were absent in the LED lamp illumination

To understand the chemical reactions taking place in the solar cells we prepared four separate samples in the following configurations;

(i.) Sample 1: FTO/TiO_2-bl/TiO_2-mp/$CH_3NH_3PbI_3$:PCBM/P3HT,
(ii.) Sample 2: FTO/TiO_2-bl/TiO_2-mp/$CH_3NH_3PbI_3$:PCBM/P3HT/Cu,
(iii.) Sample 3: FTO/TiO_2-bl/TiO_2-mp/$CH_3NH_3PbI_3$:PCBM/P3HT/Cu,
(iv.) Sample 4: FTO/TiO_2-bl/TiO_2-mp/$CH_3NH_3PbI_3$:PCBM/P3HT/Cu.

All the samples were prepared in identical conditions and Sample 2, 3 and 4 were exactly the same. The only difference in Sample 1 was that it did not have top Cu electrode. Sample 1 and 2 were stored in a dark chamber whereas Sample 3 and 4 were stored in natural conditions under direct sunlight outside the laboratory. None of these samples were encapsulated. After around 150 h of storage the top Cu electrode of Sample 4 was peeled off carefully using a cello tape. The cello tape was stick on the top of the sample and peeled off in such a way that only top Cu electrode came off with the tape not any other layer. Now all the four samples were subjected to XRD analysis to understand the chemical changes happened in them. Figure 8 shows the XRD patterns of all the four samples. The XRD peaks corresponding to different materials have been represented by different symbols shown in the inset of the figure. Sample 1 exhibited the XRD peaks at 2θ values of 14.2°, 24.6°, 26.6°, 28.6°, 32.1°, 33.9°, 37.9°, 40.7°, 43.2°, 51.6°, 54.7°, 61.7° and 65.7°. The peaks at 26.6°, 33.9°, 37.9°, 51.6°, 54.7°, 61.7° and 65.7° corresponded to FTO/TiO_2-bl/TiO_2-mp structure and the other peaks at 14.2°, 24.6°, 28.6°, 32.1°, 40.7° and 43.2° corresponded to (110), (202), (220), (310), (224) and (314) planes of $CH_3NH_3PbI_3$ perovskite. Since P3HT is an amorphous polymer and other materials are highly crystalline, the XRD features of P3HT were not visible in the XRD pattern. In case of Sample 2 we observed three additional peaks at 2θ values of 43.6°, 50.8° and 74.4° which corresponded to (111), (200) and (220) planes of the top Cu electrode. These results show that even after around 150 h of dark storage, there were no chemical reactions happened in the samples and they were just like fresh samples. It can be inferenced from these results that Cu is very stable and reacts extremely slow with perovskite film in the dark storage. But in case of Sample 3, after around 150 h of storage in natural outdoor conditions the XRD peaks at 14.2°, 24.6°, 28.6°, 32.1°, 40.7° and 43.2°, which were present in Sample 2, disappeared and new XRD peaks at 25.7°, 30.1°, 32.7° and 42.5° appeared. Disappearance of peaks at 14.2°, 24.6°, 28.6°,

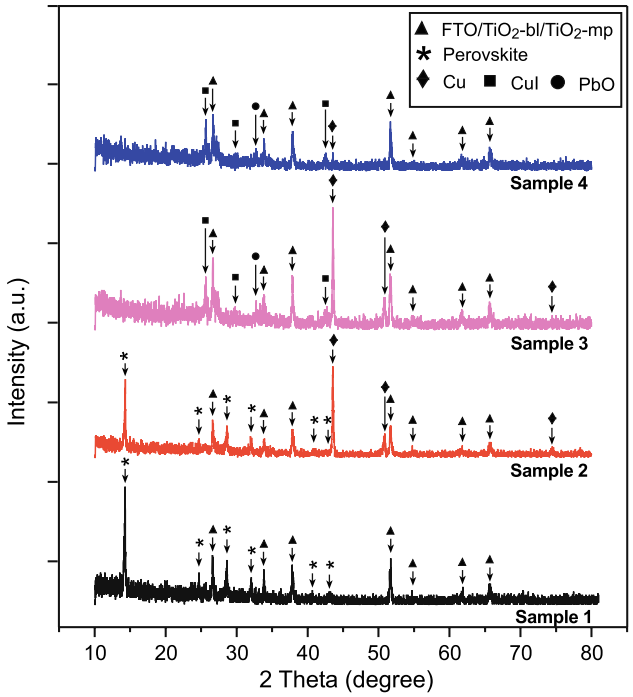

Fig. 8 XRD patterns of FTO/TiO_2-bl/TiO_2-mp/$CH_3NH_3PbI_3$:PCBM/P3HT (Sample 1), FTO/TiO_2-bl/TiO_2-mp/$CH_3NH_3PbI_3$:PCBM/P3HT/Cu (Sample 2), FTO/TiO_2-bl/TiO_2-mp/$CH_3NH_3PbI_3$:PCBM/P3HT/Cu (Sample 3) and FTO/TiO_2-bl/TiO_2-mp/$CH_3NH_3PbI_3$:PCBM/P3HT/Cu (Sample 4) after 150 h of storage. Sample 1 and 2 were stored in a dark chamber whereas Sample 3 and 4 were stored in natural conditions under direct sunlight outside the laboratory. Please note that before XRD measurements the top Cu electrode of Sample 4 had been peeled off using a cello tape

32.1°, 40.7° and 43.2° clearly indicated that perovskite had decomposed and some chemical reactions had taken place in Samples 3 that resulted in variation in its XRD pattern. More information about these chemical reactions was gathered from the XRD pattern of Sample 4, which was also stored in the same outdoor conditions along with Sample 3 but its top Cu electrode had been peeled off before XRD measurements. In case of Sample 4 we observed the XRD peaks at 2θ values of 25.7°, 26.6°, 30.1°, 32.7°, 33.9°, 37.9°, 42.5°, 43.6°, 51.6°, 54.7°, 61.7° and 65.7°. The peaks at 26.6°, 33.9°, 37.9°, 51.6°, 54.7°, 61.7° and 65.7° correspond to the FTO/TiO_2-bl/TiO_2-mp structure. The peaks at 25.7°, 30.1°, 32.7° and 42.5° were also present in Sample 3. A very little peak at 43.6° in Sample 4 corresponds to (111) plane of Cu. Though we had peeled off the top Cu electrode, yet the existence of XRD peak at 43.6° in Sample 4 indicates that Cu had diffused into the layers underneath. Now we noticed that the peaks at 25.7°, 30.1°, and 42.5° were representing (111), (200) and (220) planes of CuI. These are very interesting results and indicate that under natural outdoor conditions Cu diffuses into the layers underneath and reacts with perovskite film to form CuI. As discussed previously the $CH_3NH_3PbI_3$ perovskite is expected to decompose into CH_3NH_3I and PbI_2 where CH_3NH_3I decomposed further into CH_3NH_2 and HI [15, 16]. But we did not see any feature of PbI_2 in the XRD patterns of Sample 3 and 4 which indicated that PbI_2 also decomposed in outdoor conditions. Detailed analysis showed that the peak at 32.7° in Sample 3 and 4 corresponded to (110) plane of PbO, which means that due to very harsh environmental conditions outside, PbI_2 converted into PbO. From these investigations we can inference that under direct sunlight in natural outdoor conditions following chemical reactions take place in the Cu electrode based PSCs;

$$CH_3NH_3PbI_3 \rightarrow CH_3NH_2\uparrow + PbI_2 + HI \quad (1)$$

$$2PbI_2 + O_2 \rightarrow 2PbO + 2I_2\uparrow \quad (2)$$

$$2Cu_2 + 2HI \rightarrow 2CuI + H_2\uparrow \quad (3)$$

$$2Cu + I_2 \rightarrow 2CuI \quad (4)$$

The disappearance of top Cu electrode in the samples stored under direct sunlight was because of its reaction with perovskite and conversion into CuI.

In the storage under direct sunlight, we also observed photo-bleaching in the perovskite films caused by its photo-oxidation. The photo-bleaching could be easily seen in the non-active areas of the solar cells where there was no Cu deposition. Photo-bleaching caused the color of perovskite film to fade up. During photo-bleaching process the O_2 entities present in the system attacks on the chromophores of the perovskite and decompose them. $CH_3NH_3PbI_3$ first decomposes into CH_3NH_2, PbI_2 and HI that is followed by oxidation of CH_3NH_2 and PbI_2 to convert them into CO_2 and PbO respectively. The photo-bleaching under solar illumination was very fast compared to that under LED lamp illumination because photo-oxidation of the materials gets accelerated in the presence of ultraviolet (UV) light [32]. It is worth mentioning here that Cu also gets oxidized in the presence of O_2 and H_2O molecules through following chemical reactions;

$$4Cu + O_2 \rightarrow 2Cu_2O \quad (5)$$

$$4Cu + 2H_2O + O_2 \rightarrow 4CuOH \quad (6)$$

These Cu oxides can also react with HI through following chemical reactions and contribute to degradation in PSCs;

$$Cu_2O + 2HI \rightarrow 2CuI + H_2O \quad (7)$$

$$CuOH + HI \rightarrow CuI + H_2O \quad (8)$$

We observed oxidation of Cu electrode when some of the devices were left in air under ambient conditions (24 ± 4 °C and 45 ± 5% RH) without encapsulation. After some time we could easily see the Cu electrode getting corroded by environmental O_2 and H_2O molecules. The oxidation in Cu electrode was visible in terms of changes in its surface color

Fig. 9 Photographs of a Cu electrode based PSC taken after different time intervals. The solar cell was not encapsulated and stored in dark. The oxidation of top Cu electrode with time could be seen clearly by the change in its surface color

as shown in Fig. 9. It is therefore very important to make sure that Cu deposition is done in very high vacuum and it does not get oxidized during deposition. If there are any Cu oxides before Cu electrode in the solar cells they will create interfacial barriers and inhibit collection of holes at Cu metal contacts and the solar cells will not perform well. Cu oxides are not good for PSCs and should be avoided to form.

4 Conclusion

We have investigated the photo-stability of $CH_3NH_3PbI_3$ based PSCs with Cu as top electrode. The solar cells were prepared in normal geometry on the FTO coated glass substrates and Cu electrodes served as anode. For understanding of degradation mechanisms the solar cells were stored in different illumination conditions like in dark, under continuous illumination of a white LED lamp and under natural sunlight outside the laboratory and tested for their stability as per the ISOS-D-1, ISOS-L-1 and ISIS-O-1 protocols respectively. Under dark storage the solar cells were very stable but under continuous illumination of LED lamp the solar cells exhibited little degradation. But more interestingly under natural sunlight the solar cells degraded very fast and it was because of very severe environmental conditions outside and very strong UV and IR contents in the solar radiation. The degradation under illumination of white LED lamp or natural sunlight was mainly because of photo-oxidation of the perovskite films and their chemical reactions with Cu electrode. Though the chemical reactions were very slow in dark and under LED lamp illumination but they got accelerated under harsh outdoor conditions which led to very rapid degradation in the photovoltaic performance of the solar cells. We observed decomposition and oxidation of perovskite film, diffusion of Cu into underlying films and its chemical reactions with perovskite constituents. Though Cu electrode was expected to impart very high stability in PSCs but it also reacted with O_2, H_2O and $CH_3NH_3PbI_3$ perovskite film. From these studies we can inference that Cu too is not a very stable electrode material for PSCs in very harsh environmental conditions. Therefore to ensure very high stability in PSCs and for their commercial viability we need to find out some other suitable alternate material for electrode applications.

Acknowledgements The financial support by CSIR-India through CSIR-YSA research Grant No. (OLP-163332) is greatly acknowledged. Thanks are due to Dr. N. Vijayan and Mr. M. Saravanan of CSIR-NPL for XRD measurements and recording the SEM images of the films respectively. AKC is also thankful to CSIR, India for providing him the financial support through its Senior Research Fellowship.

References

1. M.A. Green, A. Ho-Baillie, H.J. Snaith, Nat. Photon. **8**, 506 (2014)
2. National Renewable Energy Laboratory (NREL) PV Efficiency Chart, https://www.nrel.gov/pv/assets/images/efficiency-chart.png
3. T. Duong, Y.L. Wu, H. Shen, J. Peng, X. Fu, D. Jacobs, E.C. Wang, T.C. Kho, K.C. Fong, M. Stocks, E. Franklin, A. Blakers, N. Zin, K. McIntosh, W. Li, Y.B. Cheng, T.P. White, K. Weber, K. Catchpole, Adv. Energy Mater. **7**(14), 1–11 (2017). https://doi.org/10.1002/aenm.201700228
4. K.A. Bush, A.F. Palmstrom, Z.J. Yu, M. Boccard, R. Cheacharoen, J.P. Mailoa, D.P. McMeekin, R.L.Z. Hoye, C.D. Bailie, T. Leijtens, I.M. Peters, M.C. Minichetti, N. Rolston, R. Prasanna, S. Sofia, D. Harwood, W. Ma, F. Moghadam, H.J. Snaith, T. Buonassisi, Z.C. Holman, S.F. Bent, M.D. McGehee, Nat. Energy **2**, 17009 (2017)
5. J. Werner, L. Barraud, A. Walter, M. Brauninger, F. Sahli, D. Sacchetto, N. Tetreault, B.P. Salomon, S.J. Moon, C. Allebe, M. Despeisse, S. Nicolay, S. De Wolf, B. Niesen, C. Ballif, ACS Energy Lett. **1**, 474 (2016)
6. P. Loper, B. Niesen, S.J. Moon, S. Martin de Nicolas, J. Holovsky, Z. Remes, M. Ledinsky, F.J. Haug, J.H. Yum, S.D. Wolf, C. Ballif, IEEE J. Photovolt. **4**, 1545 (2014)
7. J.E. Bishop, T.J. Routledge, D.G. Lidzey, J. Phys. Chem. Lett. **9**, 1977 (2018)
8. Y. Deng, Q. Dong, C. Bi, Y. Yuan, J. Huang, Adv. Energy Mater. **6**, 1600372 (2016)
9. J.B. Whitaker, D.H. Kim, B.W. Larson, F. Zhang, J.J. Berry, M.F.A.M. van Hest, K. Zhu, Sustain. Energy Fuels **2**, 2442 (2018)
10. Y. Rong, Y. Ming, W. Ji, D. Li, A. Mei, Y. Hu, H. Han, J. Phys. Chem. Lett. **9**, 2707 (2018)
11. J.H. Kim, S.T. Williams, N. Cho, C.C. Chueh, A.K.Y. Jen, Adv. Energy Mater. **5**, 1401229 (2015)
12. T. Leijtens, G.E. Eperon, N.K. Noel, S.N. Habisreutinger, A. Petrozza, H.J. Snaith, Adv. Energy Mater. **5**, 1500963 (2015)
13. J. Yang, B.D. Siempelkamp, D. Liu, T.L. Kelly, ACS Nano **9**, 1955 (2015)
14. D. Wang, M. Wright, N.K. Elumalai, A. Uddin, Sol. Energy Mater. Sol. Cells **147**, 255 (2016)
15. G. Niu, X. Guo, L. Wang, J. Mater. Chem. A **3**, 8970 (2015)
16. J.M. Frost, K.T. Butler, F. Brivio, C.H. Hendon, M. van Schilfgaarde, A. Walsh, Nano Lett. **14**, 2584 (2014)
17. B. Coning, J. Drijkoningen, N. Gauquelin, A. Babayigit, J. D'Haen, L. D'Olieslaeger, A. Ethirajan, J. Verbeeck, J. Manca, E. Mosconi, F. De Angelis, H.G. Boyen, Adv. Energy Mater. **5**, 1500477 (2015)
18. I.C. Smith, E.T. Hoke, D.S. Ibarra, M.D. McGehee, H.I. Karunadasa, Angew Chem. Int. Ed. **53**, 11232 (2014)
19. I.C. Smith, E.T. Hoke, D.S. Ibarra, M.D. McGehee, H.I. Karunadasa, Angew Chem. Int. Ed. **126**, 11414 (2014)

20. Z. Yang, A. Rajagopal, S.B. Jo, C.C. Chueh, S. Williams, C.C. Huang, J.K. Katahara, H.W. Hillhouse, A.K.Y. Jen, Nano Lett. **16**, 7739 (2016)
21. D.P. McMeekin, G. Sadoughi, W. Rehman, G.E. Eperon, M. Saliba, M.T. Hörantner, A. Haghighirad, N. Sakai, L. Korte, B. Rech, M.B. Johnston, L.M. Herz, H.J. Snaith, Science **351**, 151 (2016)
22. M. Saliba, T. Matsui, J.Y. Seo, K. Domanski, J.P.C. Baena, M.K. Nazeeruddin, S.M. Zakeeruddin, W. Tress, A. Abate, A. Hagfeldt, M. Grätzel, Energy Environ. Sci. **9**, 1989 (2016)
23. X. Li, M.I. Dar, C. Yi, J. Luo, M. Tschumi, S.M. Zakeeruddin, M.K. Nazeeruddin, H. Han, M. Grätzel, Nat. Chem. **7**, 703 (2015)
24. A.K. Chauhan, P. Kumar, J. Phys. D Appl. Phys. **50**, 325105 (2017)
25. A.K. Chauhan, P. Kumar, S.R. Pal, S.K. Srivastava, S. Muthiah, J. Mater. Sci. **52**, 10886 (2017)
26. Y. Kato, L.K. Ono, M.V. Lee, S. Wang, S.R. Raga, Y. Qi, Adv. Mater. Interfaces **2**, 1500195 (2015)
27. E.M. Sanehira, B.J.T. de Villers, P. Schulz, M.O. Reese, S. Ferrere, K. Zhu, L.Y. Lin, J.J. Berry, J.M. Luther, ACS Energy Lett. **1**, 38 (2016)
28. J. You, L. Meng, T.B. Song, T.F. Guo, Y. Yang, W.H. Chang, Z. Hong, H. Chen, H. Zhou, Q. Chen, Y. Liu, N. De Marco, Y. Yang, Nat. Nanotechnol. **11**, 75 (2016)
29. J. You, L. Meng, T.B. Song, T.F. Guo, Y.M. Yang, W.H. Chang, Z. Hong, H. Chen, H. Zhou, Q. Chen, Nat Nanotechnol **11**, 75 (2016)
30. J. Zhao, X. Zheng, Y. Deng, T. Li, Y. Shao, A. Gruverman, J. Shield, J. Huang, Energy Environ. Sci. **9**, 3650 (2016)
31. R.W. Revie, H.H. Uhlig, *Corrosion and Corrosion Control* (Wiley, Hoboken, 2008)
32. P. Kumar, *Organic Solar Cells: Device Physics, Processing, Degradation and Prevention* (CRC Press, New York, 2016)
33. D.K. Chaudhary, P. Kumar, L. Kumar, Chem. Phys. Lett. **685**, 210 (2017)
34. C.H. Chiang, C.G. Wu, Nat. Photon. **10**, 196 (2016)
35. D. Bi, W. Tress, M.I. Dar, P. Gao, J. Luo, C. Renevier, K. Schenk, A. Abate, F. Giordano, J.P.C. Baena, J.D. Decoppet, S.M. Zakeeruddin, M.K. Nazeeruddin, M. Grätzel, A. Hagfeldt, Sci. Adv. **2**, e1501170 (2016)
36. M. Saliba, S. Orlandi, T. Matsui, S. Aghazada, M. Cavazzini, J.P. Correa-Baena, P. Gao, R. Scopelliti, E. Mosconi, K.H. Dahmen, F.D. Angelis, A. Abate, A. Hagfeldt, G. Pozzi, M. Graetzel, M.K. Nazeeruddin, Nat. Energy **1**, 15017 (2016)
37. D. Angmo, F.C. Krebs, Energy Technol. **3**, 774 (2015)
38. P. Vivo, J.K. Salunke, A. Priimagi, Materials **10**, 1087 (2017)
39. C.H. Chiang, C.G. Wu, Nat. Photon. **10**, 196 (2016)
40. G.E. Eperon, V.M. Burlakov, P. Docampo, A. Goriely, H.J. Snaith, Adv. Funct. Mater. **24**, 151 (2014)
41. F. Zabihi, MdRA Yazdi, M. Eslamian, Nanoscale Res. Lett. **11**, 71 (2016)
42. W. Zhou, Y. Zhao, C. Shi, H. Huang, J. Wei, R. Fu, K. Liu, D. Yu, Q. Zhao, J. Phys. Chem. C **120**, 4759 (2016)
43. P. Kumar, S.C. Jain, H. Kumar, S. Chand, V. Kumar, Appl. Phys. Lett. **94**, 183505 (2009)
44. M.V. Khenkin, K.M. Anoop, I.V. Fisher, S. Kolusheva, Y. Galagan, F. Di Giacomo, O. Vukovic, B.R. Patil, G. Sherafatipour, V. Turkovic, H.G. Rubahn, M. Madsen, A.V. Mazanik, E.A. Katz, A.C.S. Appl, Energy Mater. **1**, 799 (2018)